ACS Photonics

Article

pubs.acs.org/journal/apchd5

Configurable Plasmonic Band-Pass Filters Operating under the Addition Rule

Jisoo Kyoung* and Sung Woo Hwang

Samsung Advanced Institute of Technology, Samsung Electronics Co., Suwon-si 443-803, Korea

ABSTRACT: Optical filters are one of the essential optical elements in telecommunication systems, signal processing devices, and spectrometers. The design principle of conventional filters is based on the classical theory of optics; for example, the transfer-matrix method is applied in Fabry−Pérot cavities. Because of their large thickness, such filters follow the multiplication rule of probability: if light passes through the two filters in turn, the final transmission spectrum is the product of the two individual spectra. This property makes it difficult to design a new filter having multipass-bands because such a filter cannot be constructed from a combination of the existing filters having single pass-band. Here we propose an alternative type of band-pass filter that operates under the addition rule of probability, wherein the final transmission spectrum is simply the sum of the individual spectra. We show that the strong plasmonic coupling between the slits and heterostructured epsilon-near-zero (ENZ) films gives rise to the addition rule. Therefore, a filter with a desired transmission spectrum can be easily configured from a combination of well-known filters. We demonstrate that the narrow bandwidth of the ENZ materials and plasmonic distant coupling between the slits and ENZ film contribute to the *mutually exclusive* condition for the addition rule. Furthermore, through developing an LC circuit model for the band-pass filters, we succeed in predicting the resonance positions in the transmission spectra. We believe that our novel findings can pave the way toward overcoming the current limitations of filter technologies by significantly reducing the time required to design and manufacture optical filters.

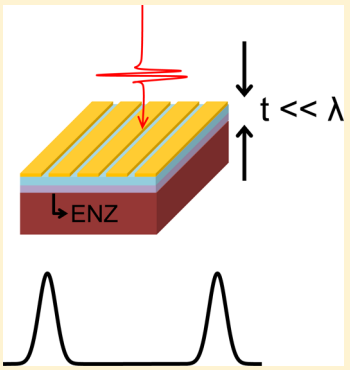

KEYWORDS: *mid-IR, optical filter, epsilon-near-zero, addition rule, slit, configurable*

Recently, the mid-infrared (mid-IR) light source has attracted significant attention because it contains the characteristic vibrational modes of the most common molecules such as carbon dioxide, ethylene, ammonia, and glucose.[1,2] This renders the mid-IR source essential for applications related to harmful gas detectors, medical diagnostics, as well as chemical sensors and biosensors. Moreover, the transmission windows of Earth's atmosphere in the mid-IR range, 3−5 and 8−13 μm, are important for free-space communications, IR countermeasures, and fire monitoring. To fully utilize the advantages of the mid-IR source, high-performance optical elements such as lenses, polarizers, beam splitters, and filters are crucial. Conventionally, mid-IR filters have consisted of dielectric layers with alternating high and low refractive indices (Figure 1a).[3,4] The operating principle of the dielectric multilayer filters is based on light transmission, reflection, and interference phenomena, which can be easily understood through Fresnel formulas and geometrical optics.[5] However, in order to achieve the desired performance, several tens of dielectric films are utilized and therefore the total thickness of the filter is usually greater than the target wavelengths.

From the perspective of a photon, a band-pass filter can be regarded as a kind of potential barrier, and then the transmission coefficient indicates the transmission probability. Let us suppose that a photon is passing through two band-pass filters sequentially. The final output transmission probability would follow the multiplication rule of probability because the two events are *mutually independent*. Figure 1a summarizes the behavior of classical filters operating under the multiplication rule. The orange and magenta lines represent the virtual transmission spectra through the filters 1 and 2, respectively, and the black lines are the product of the two spectra. If the transmission bands are completely separated, the detector would be entirely dark (top panel). However, when an intersection exists between the two pass-bands, only a small amount of light in the overlapping region can pass through both filters (bottom panel). Because of the multiplication rule, a new functional filter having multipass-bands cannot be constructed from a combination of pre-existing filters having single pass-band, which makes it difficult to design and manufacture a new multilayer filter even though the underlying physics is simple. Accordingly, a natural question arises: is it possible to construct band-pass filters that operate under the addition rule of probability instead of the multiplication rule?

Recently, it has been reported that epsilon-near-zero (ENZ) materials can be employed to enhance the wave transmission through a single subwavelength aperture in a flat screen.[6−10] This is because the zero permittivity of the ENZ film increases the coupling efficiency between the light and the small aperture and, furthermore, induces a high concentration of the local electromagnetic energy inside the hole.[11] In this work, we introduce a new type of mid-IR band-pass filter constructed

Received: January 11, 2016
Published: April 20, 2016

DOI: 10.1021/acsphotonics.6b00019
ACS Photonics 2016, 3, 819−827

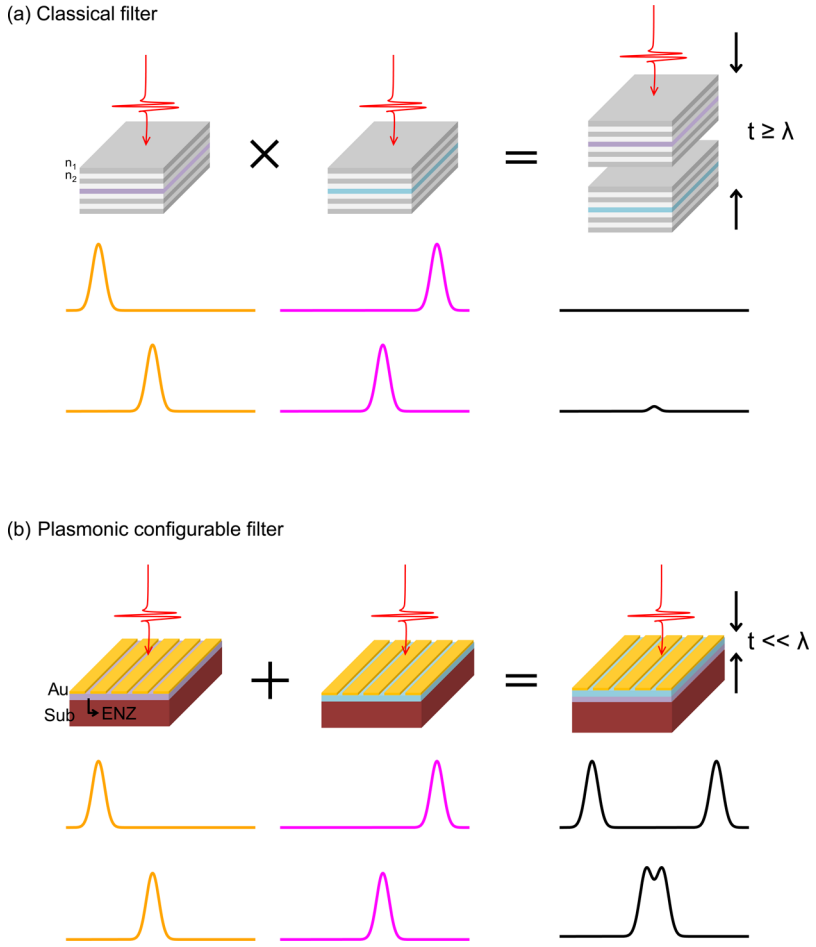

Figure 1. (a) Classical filters operating under the multiplication rule of probability. (b) Plasmonic configurable filters based on the slits and epsilon-near-zero (ENZ) heterostructures operating under the addition rule of probability.

from Au nanoslits on an ENZ thin film (Figure 1b), which allows for a single sharp transmission peak at the ENZ position. We also show that the novel band-pass filter follows the addition rule of probability when vertically stacked multi-heterostructures of ENZ materials are utilized instead of a single layer (Figure 1b, lower panel); in this way the final transmission probability simply becomes the sum of the two individual probabilities, as illustrated in the bottom part of the Figure 1b (orange and magenta lines, virtual transmission through the slit on a single ENZ film; black lines, the sum of the orange and magenta curves). In order to apply the addition rule, the two events should be *mutually exclusive*. In our case, two factors are responsible for this condition of mutual exclusivity: the narrow ENZ bandwidth and the ultralow filter thickness. Apart from the narrow anomalous dispersion, the ENZ materials work as ordinary dielectrics; in this manner, the incident light can exclusively interact with each ENZ layer. In addition, because the total thickness of the ENZ hetero-structures lies in the deep subwavelength regime of $\sim \lambda/20$, the near-field coupling of the slit and the distant ENZ materials is still strong, which allows for multiband transmission. We theoretically and experimentally demonstrate that, on account of the addition rule of our ENZ based filters, the pass-bands can be easily configured from the previously known pass-bands of existing filters.

First, we discuss the transmission characteristics of the band-pass filter consisting of slit arrays on a single ENZ layer, which is the building block for multilayer systems. The Lorentz phonon oscillator model for the dielectric function has successfully explained the optical properties of the ionic crystal near the phonon band. After solving the equations of the ions' motion, the dielectric constant is given by[12]

$$\frac{\varepsilon(\nu)}{\varepsilon_\infty} = 1 + \frac{\nu_{LO}^2 - \nu_{TO}^2}{\nu_{TO}^2 - i\nu\gamma - \nu^2} \quad (1)$$

where ν_{TO} and ν_{LO} are the transverse and longitudinal optical phonon wavenumbers, respectively, and γ is the damping coefficient. The damping coefficient is generally small compared to the transverse phonon wavenumber or the resonant wavenumber. This means that ε vanishes approximately at the longitudinal phonon wavenumber, $\nu = \nu_{LO}$, which is the naturally occurring ENZ position. The calculated real and imaginary dielectric constants for nine different ENZ materials with various TO phonon frequencies are plotted in Figure 2a and b when $\varepsilon(0) = 3.22$, $\varepsilon_\infty = 2.44$, and $\gamma = 400\ \mathrm{cm}^{-1}$. In fact, for each graph in Figure 2a, there exist two permittivity zero points; one is in the anomalous dispersion band that is associated with a decrease in Re $\varepsilon(\nu)$ with ν, whereas the other is located at the LO phonon wavenumber. The zero permittivity in the anomalous dispersion is not an ENZ point owing to the large imaginary part of the dielectric constant (Figure 2b). Even though the dielectric constants in Figure 2a,b are mathematically generated according to eq 1, they can

DOI: 10.1021/acsphotonics.6b00019
ACS Photonics 2016, 3, 819−827

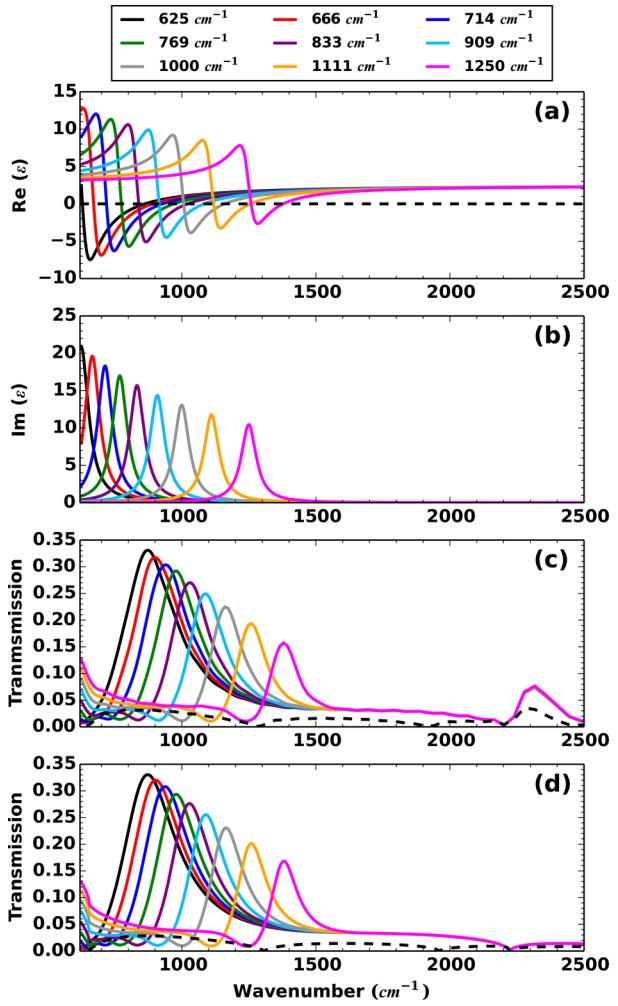

Figure 2. (a) Real and (b) imaginary parts of the dielectric constant for various epsilon-near-zero (ENZ) materials. The legend represents the transverse optical (TO) phonon wavenumbers for ENZ materials. (c) Transmission spectra through the band-pass filter calculated by finite difference time domain (FDTD) simulations. Dashed line: Si substrate without the ENZ film. (d) Transmission spectra through the band-pass filter calculated by the analytic model (eq 2). Dashed line: Si substrate without the ENZ film.

describe the behavior of the realistic ionic crystals quite well, which have natural ENZ points at LO phonon frequencies.[13−15]

Finite difference time domain (FDTD) simulations (FDTD Solutions, Lumerical Solutions, Inc., Canada) were then carried out to calculate the transmission through the ENZ band-pass filters. The simulations were performed under the two-dimensional configuration (cross sectional view of the slit) with the periodic boundary condition along the lateral axis. The material of the slit arrays was set as Au; the thickness, width, and period were 70 nm, 500 nm, and 4.5 μm, respectively. Undoped Si constitutes an appropriate substrate because no absorption band exists in the mid-IR range. The thickness of the substrate was 50 μm, which was sufficiently large compared to the wavelength (4−16 μm or 625−2500 cm^{-1} wavenumbers); the transmission monitor was located outside the substrate. Finally, the 300 nm thick ENZ film was inserted between the slits and the Si substrate. We used the dielectric constants of Au and Si provided by the software, whereas that of ENZ film was newly imported according to the results of Figure 2a,b. The magnitude of the incident electric field was set as 1 V/m. The transmission spectra consisted of the narrow and strong peaks with thin ENZ films, as shown in Figure 2c, while only a negligible amount of transmission was observed with only the Si substrate (dashed line). The peak value decreases as the TO phonon wavenumber increases because of the $1/f$ transmission characteristic of the slit.[16]

In order to understand the mechanisms of the resonant transmission, the electric near-field distributions on the cross-sectional area of the sample are illustrated in Figure 3. Figure 3a and b correspond to the ENZ film (ENZ position: 869 cm^{-1} or ν_{TO} = 625 cm^{-1}) at the incident wavenumbers 869 and 1250 cm^{-1}, respectively, whereas Figure 3c,d corresponds to the ENZ film whose zero permittivity position is located at 1250 cm^{-1}. The total monitor size is 5 μm × 5 μm and all color bars are scaled from 0 to 10 for ease of comparison. As can be clearly seen, strong near-field enhancements are observed when the incident wavenumbers are matched to the ENZ positions (Figure 3a,d), which means that the electric field enhancements are originated from the ENZ effect. Recently, our group shows that an ENZ material can work as a magnetic mirror (the light reflects back at the ENZ surface keeping the direction of the electric field) and induce an order of electric field enhancement at the plasmonic gap compared to the ordinary substrate.[11] Large electric field enhancement in the vicinity of the metallic gaps can be used in lowering the critical temperature of the insulator-to-metal phase transition, quantum plasmonic tunneling, and transmission modulation.[17−19]

Owing to the simple geometry of our band-pass filters, analytical calculation of the transmission spectra is possible under the assumption that the thin metal slits are made of perfect electric conductors, and that the single-mode approximation is valid inside the subwavelength aperture.[20] By modal expansion of the electromagnetic fields and appropriate boundary matching at the interfaces, we can obtain the zeroth-order transmission as follows:[21]

$$T_0 = \left(\frac{w}{p}\right)^2 \left|\frac{2}{W^1 + W^3}\right|^2 \times \left|\frac{1}{\frac{1}{n_{Si}}\cos(n_{ENZ}kd) - i\frac{1}{n_{ENZ}}\sin(n_{ENZ}kd)}\right|^2 \left(\frac{2}{1 + n^{Si}}\right)^2 \quad (2)$$

where w is the slit width, p is the slit period, d is the thickness of the ENZ film, and k is the wavevector of the incident light. n_{ENZ} and n_{Si} indicate the refractive indices of ENZ and Si materials, respectively. The denominator W^1 and W^3 mean the self-illuminations of the hole[22] via vacuum and substrate modes, which are defined as follows:

$$W^1 = \frac{w}{p}k\sum_m \frac{\mathrm{sinc}^2\left(\frac{wk_m}{2}\right)}{\kappa_m^1} \quad (3)$$

$$W^3 = \varepsilon_{ENZ}\frac{w}{p}k\sum_m \frac{\mathrm{sinc}^2\left(\frac{wk_m}{2}\right)}{\kappa_m^{n_{ENZ}}} \frac{\left(\frac{\kappa_m^{n_{ENZ}}}{\varepsilon_{ENZ}}\cos(\kappa_m^{n_{ENZ}}d) - i\frac{\kappa_m^{n_{Si}}}{\varepsilon_{Si}}\sin(\kappa_m^{n_{ENZ}}d)\right)}{\left(-i\frac{\kappa_m^{n_{ENZ}}}{\varepsilon_{ENZ}}\sin(\kappa_m^{n_{ENZ}}d) + \frac{\kappa_m^{n_{Si}}}{\varepsilon_{Si}}\cos(\kappa_m^{n_{ENZ}}d)\right)} \quad (4)$$

with $k_m = 2\pi m/p$, $\kappa_m^{n_i} = \sqrt{n_i^2k^2 - k_m^2}$. Remarkably, the calculated zeroth-order transmission spectra (Figure 2d) for various band-pass filters are quite similar to the FDTD results (Figure

DOI: 10.1021/acsphotonics.6b00019
ACS Photonics 2016, 3, 819−827

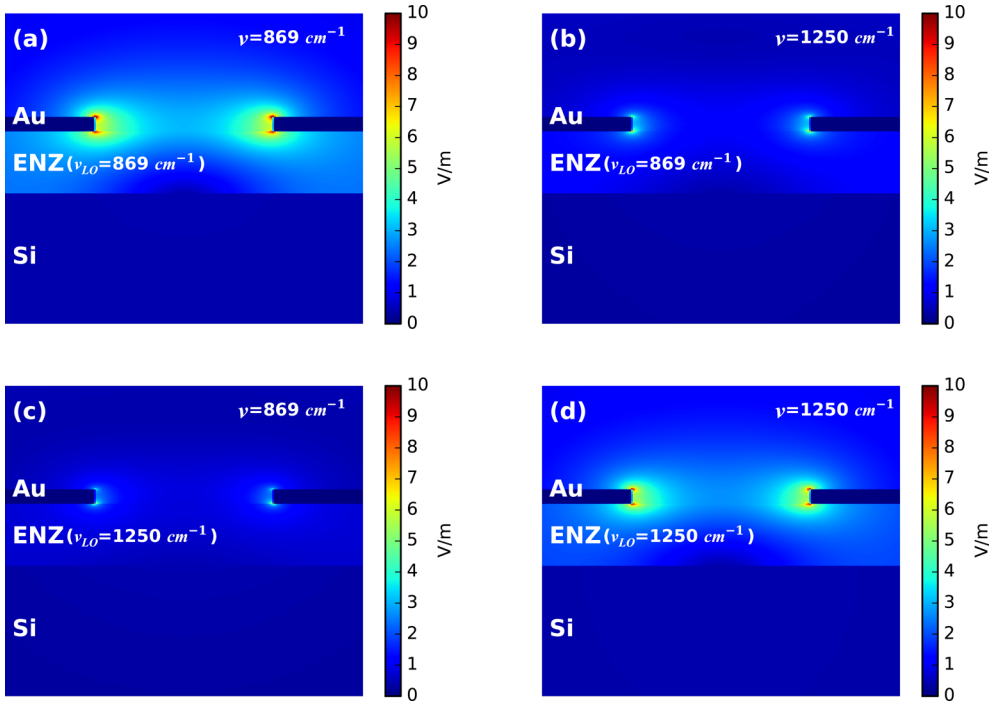

Figure 3. Near field distribution of the band-pass filter with the epsilon-near-zero (ENZ) film (ν_{LO} = 869 cm^{-1}) at a wavenumber of (a) 869 and (b) 1250 cm^{-1}. Near-field distribution with the ENZ film (ν_{LO} = 1250 cm^{-1}) at a wavenumber of (c) 869 and (d) 1250 cm^{-1}. Strong near-field concentration is observed only when the longitudinal optical (LO) phonon wavenumber and incident light wavenumber are matched.

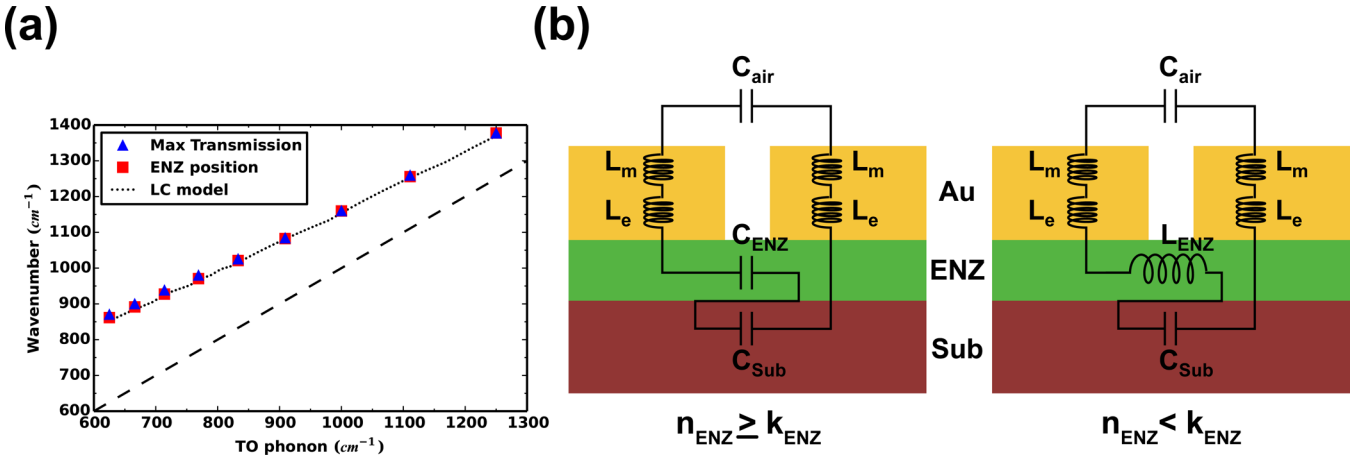

Figure 4. (a) Maximum transmission wavenumbers (blue triangles) from the spectra in Figure 1c and epsilon-near-zero (ENZ) positions (red rectangles) from Figure 1a vs transverse optical (TO) phonon wavenumbers. Excellent agreement indicates that the strong resonant transmission originates from the ENZ effect. Dotted line: predicted maximum transmission wavenumbers by our LC model. Dashed line: identity line ($y = x$ line) for comparison. (b) LC circuit model for plasmonic band-pass filters.

2c). This means that our two assumptions (namely, that Au can be regarded as a perfect conductor and that only the single mode is dominant inside the slit) are acceptable and that the zeroth-order transmission is sufficient for explaining the FDTD simulations. Actually, the permittivity of the Au at 1500 cm^{-1} wavenumber is about $-1500 + 500i$, which is sufficiently large to be considered as a perfect electric conductor.[23] It should be noted that we did not use any fitting parameters in calculating the transmission.

Each term in the right-hand side of eq 2 has a physical meaning: the first term is a geometrical factor for the ratio of the opened area to the closed area; the second term represents the total self-illumination effect of the slits; the third term represents the cavity effect that derives from the finite thickness of the ENZ film; and the last term is inserted to calculate the electric field outside the Si substrate. The first and last terms are constants (we fixed the refractive index of Si as 3.4.); the variation of the third term along the wavenumber is small because it consists of sine and cosine functions, and the thickness of the ENZ film is much smaller than the wavelength, $d/\lambda \sim 20$. Thus, it is probably the second term of eq 2 that leads the drastic changes of the transmission in Figure 2d. Since the self-illumination term lies in the denominator, the maximum transmission would be observed at the minimum total self-illumination point. W^1 varies little as the wavenumber increases, whereas the real and imaginary parts of W^3 become very small when the ε_{ENZ} approaches zero, according to eq 4. Therefore, we may conclude that the peak position of the

DOI: 10.1021/acsphotonics.6b00019
ACS Photonics 2016, 3, 819−827

transmission band would be observed around the ENZ point. Figure 4a shows the positions of the maximum transmission (blue triangles) taking from the FDTD simulation (Figure 2d) and the corresponding ENZ positions (red squares) of the various ENZ materials. As clearly seen, two data are remarkably well matched, indicating that the maximum transmission originated from the ENZ effect as discussed above.

As illustrated in Figure 3, the electric field is strongly localized in the slit under resonance conditions, and the induced electric current circulates around the metal strip. In this regard, the considered structure can be approximated as a collection of local capacitors and inductors. Hence, the resonance condition for the fundamental mode of the electric response can be predicted by the equivalent LC circuit model, as sketched in Figure 4b.[24−27] For the slit array, the capacitance between the left and right strips can be approximated as a parallel-plate capacitor, described by the equation

$$C = \frac{\varepsilon_d \varepsilon_0 h l}{w} \tag{5}$$

where ε_d is the relative permittivity of the filling dielectric, ε_0 is the vacuum permittivity, h is the thickness of the metal, and l is the strip length. In our case, $\varepsilon_d = 1$ for C_{air} and 3.4 for C_{sub}. The inductance of the metal consists of two contributions. The first is the mutual inductance of the two parallel strips, which can be expressed as

$$L_m = \frac{1}{2}\frac{\mu_0 h w}{l} \tag{6}$$

where μ_0 is the vacuum permeability. The other, referred to as kinetic inductance, originates from the drifting electrons in metal, and is given by

$$L_e = \frac{h}{\varepsilon_0 \omega_p^2 \delta l} \tag{7}$$

in which $\omega_p = 1.38 \times 10^{16}$ rad/s is the plasma frequency of Au. The δ represents the skin depth of the metal film, which is on the order of 10 nm in the mid-IR range. Because most of the induced electric current flows within the skin depth δ limit, δl represents the effective cross-sectional area of the metal strip. Furthermore, the ENZ film works as a capacitor, described by the equation

$$C_{ENZ} = \frac{\varepsilon_{ENZ} \varepsilon_0 h l}{w} \tag{8}$$

when $n_{ENZ} \geq k_{ENZ}$ (left panel in Figure 4b) or an inductor, described by the equation

$$L_{ENZ} = \frac{p}{\varepsilon_{ENZ} \varepsilon_0 \omega^2 d l} \tag{9}$$

in which ω is the angular frequency of the incident wave, when $n_{ENZ} < k_{ENZ}$ (right panel in Figure 4b).[28,29] Therefore, the total impedance (Z_{tot}) of the circuit can be expressed in the following form:

$$Z_{tot} = \frac{1}{i}\left(\frac{1}{\omega C_{air}} - 2\omega L_m - 2\omega L_e + \frac{1}{\omega C_{ENZ}} + \frac{1}{\omega C_{sub}}\right)$$

$$\text{for} \quad n_{ENZ} \geq k_{ENZ}$$

$$Z_{tot} = \frac{1}{i}\left(\frac{1}{\omega C_{air}} - 2\omega L_m - 2\omega L_e - \omega L_{ENZ} + \frac{1}{\omega C_{sub}}\right)$$

$$\text{for} \quad n_{ENZ} < k_{ENZ} \tag{10}$$

The frequency that results in zero total impedance of the circuit is the resonance wavenumber of the transmission. Remarkably, our simple LC circuit model predicts the resonance wavenumber quite well, as clearly demonstrated in Figure 4a (dotted line). It should be noted that we did not use any fitting parameters in eq 5. This leads to the statement that the strongly localized surface plasmon together with the ENZ effect plays a crucial role in the resonance transmission of our band-pass filter.

The transmission intensity at resonance usually depends on the thickness of the ENZ film because a film that is too thin is negligible, whereas a film that is too thick leads to significant loss. For the sake of studying the thickness dependence, FDTD simulations were carried out for several ENZ films by varying their thicknesses. We found that the resonance positions were almost independent of the ENZ film thickness. This is because it is the refractive indices of the surrounding medium that determines the peak position rather than the thicknesses of the substrates. In all cases, the transmission at resonance (maximum transmission) shows a gentle hill shape that reaches a maximum at a certain thickness (Figure 5). This indicates that

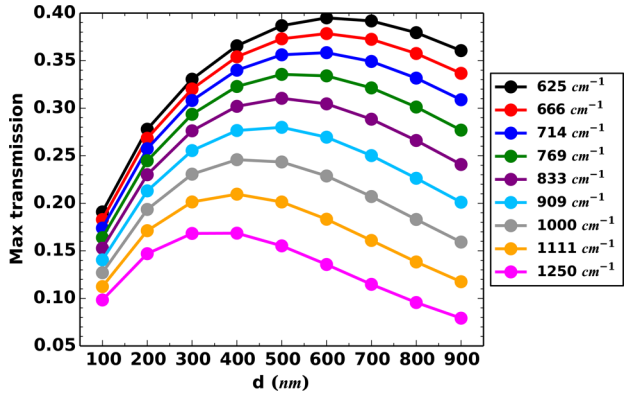

Figure 5. Transmission at resonance (maximum transmission) as a function of the epsilon-near-zero (ENZ) thickness. The legend represents the transverse optical (TO) phonon wavenumbers for ENZ materials.

the total transmission through the filter can be adjusted simply by tuning the ENZ film thickness. Meanwhile, the band-pass filters that consist of the ENZ material with a lower (higher) TO phonon wavenumber requires thicker (thinner) ENZ films to reach the maximum possible transmission (Figure 5). In addition, the resonance wavenumber is longer (shorter) for the higher (lower) TO phonon ENZ films (Figures 2c,d). Hence, we may conclude that it is the ratio between the thickness and the wavenumber that is the key parameter in determining the transmission, rather than the absolute value of the thickness itself.

In order to show the addition rule of our filter (Figure 1b), we prepare vertically stacked two ENZ films having different TO phonon wavenumbers. The insets in Figure 6a,b represent the specific configurations of the multilayered ENZ films in which the numbers represent the TO phonon wavenumbers of each ENZ material. The slits are located on the top ENZ layers.

DOI: 10.1021/acsphotonics.6b00019
ACS Photonics 2016, 3, 819−827

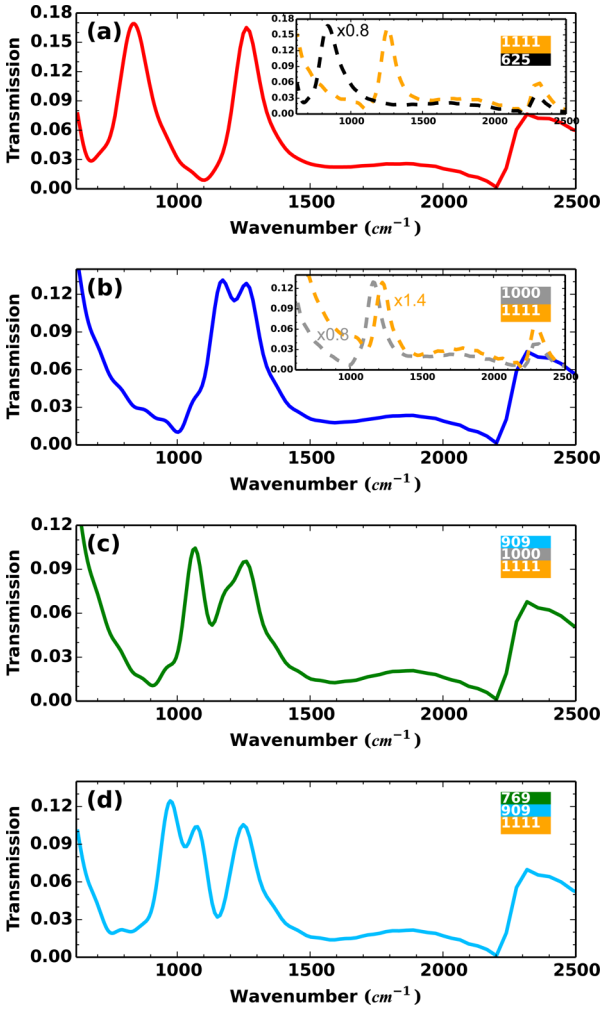

Figure 6. Calculated transmission spectra through the band-pass filters with heterostructured epsilon-near-zero (ENZ) films. The colored rectangles in the insets show the specific configurations of heterostructured ENZ films in which the numbers represent the TO phonon wavenumbers of each ENZ material. The slits are placed on the top of the rectangles. Thickness of each film: (a) 1111 cm^{-1}/300 nm, 625 cm^{-1}/180 nm, (b) 1000 cm^{-1}/250 nm, 1111 cm^{-1}/300 nm, (c) 909 cm^{-1}/150 nm, 1000 cm^{-1}/150 nm, 1111 cm^{-1}/400 nm, and (d) 769 cm^{-1}/100 nm, 909 cm^{-1}/150 nm, 1111 cm^{-1}/400 nm. The insets in figures (a) and (b): the transmission spectra for the single ENZ slab keeping the same geometry and materials parameters as in the stacked configuration. (Inset (a): orange (black) line represents transmission spectrum when the ν_{TO} = 625 cm^{-1} (ν_{TO} = 1111 cm^{-1}) ENZ slab is replaced by the ε = 3.22 dielectric. Inset (b): orange (gray) line represents transmission spectrum when the ν_{TO} = 1000 cm^{-1} (ν_{TO} = 1111 cm^{-1}) ENZ slab is replaced by the ε = 3.22 dielectric. The colored numbers are the magnification ratio of the spectra.)

To achieve the spectrum as in the conceptual diagram in Figure 1b, we select ENZ films with ν_{TO} = 1111 cm^{-1} and ν_{TO} = 625 cm^{-1} to obtain two separate peaks (Figure 6a) and ν_{TO} = 1000 cm^{-1} and ν_{TO} = 1111 cm^{-1} for mixed pass band spectrum (Figure 6b). Furthermore, referring to the result in Figure 5, the thicknesses of the individual ENZ films are delicately adjusted so that the transmissions of each band are almost equal. The transmission spectra for the filters of the two ENZ films are displayed in Figure 6a,b, for which the two ENZ positions are (a) far apart and (b) adjacent. Two individual peaks are clearly observable and the each peak position is nearly the same as the one with ENZ single layer case (Figure 2c), which means that our novel filters truly follow the addition rule of probability. To support this statement, the transmission spectra for the isolated films forming the two layer devices are displayed in the insets of the Figure 6a,b. For the single slab calculations, the same geometric and material parameters were kept as in the stacked configurations. The orange (orange) and black (gray) lines in the inset of the Figure 6a and b represent transmission spectra for the single the ν_{TO} = 1111 cm^{-1} (ν_{TO} = 1111 cm^{-1}) and ν_{TO} = 625 cm^{-1} (ν_{TO} = 1000 cm^{-1}) ENZ slabs, respectively. The colored numbers are the magnification ratio of the spectra. As mentioned above, the two positions of the transmission resonances for isolated films are well-matched with them for the heterostructured devices because the ENZ positions are unchanged during the stacking. This comparison shows exactly to what extent the position of the transmission resonances remains unaffected once the films are coupled. On the other hand, the transmission height can be different according to the dielectric environments. However, the desired transmission height is able to be easily adjusted by tuning the ENZ film thickness (Figure 5) so that the two transmission peaks are the same level. We can even extend our approach to three ENZ heterostructures (Figure 6c,d). Owing to the addition rule, the bandwidth of our band-pass filters is easily tunable. Moreover, certain bands can be blocked out of the broad spectrum depending on the ENZ film configuration.

To understand the underlying physics in the addition rule, it is worthwhile to investigate how far the interaction between the slits and ENZ materials extends. As discussed earlier, the strong near field coupling between the slits and the ENZ film plays a crucial role in sharp resonant transmission through our band-pass filters. With the aim of estimating the coupling distance systematically, we inserted an air gap between the slits and the 300 nm thick ENZ films, and calculated the transmission at resonance (maximum transmission) by changing the air gap thickness (Figure 7). The deviations of the peak positions with respect to the air gap distances were negligibly small, less than 5%, indicating that the resonance frequencies were mainly determined by the properties of the ENZ films themselves not by the geometrical configurations. Remarkably, a large amount of light can still pass through the subwavelength apertures until

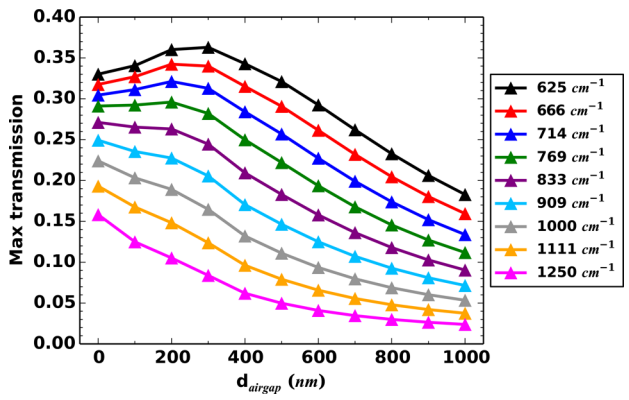

Figure 7. Transmission at resonance (maximum transmission) as a function of the air gap thickness. The air gap is placed between the slits and the 300 nm thick epsilon-near-zero (ENZ) materials. The legend represents the transverse optical (TO) phonon wavenumbers for ENZ materials.

DOI: 10.1021/acsphotonics.6b00019
ACS Photonics 2016, 3, 819–827

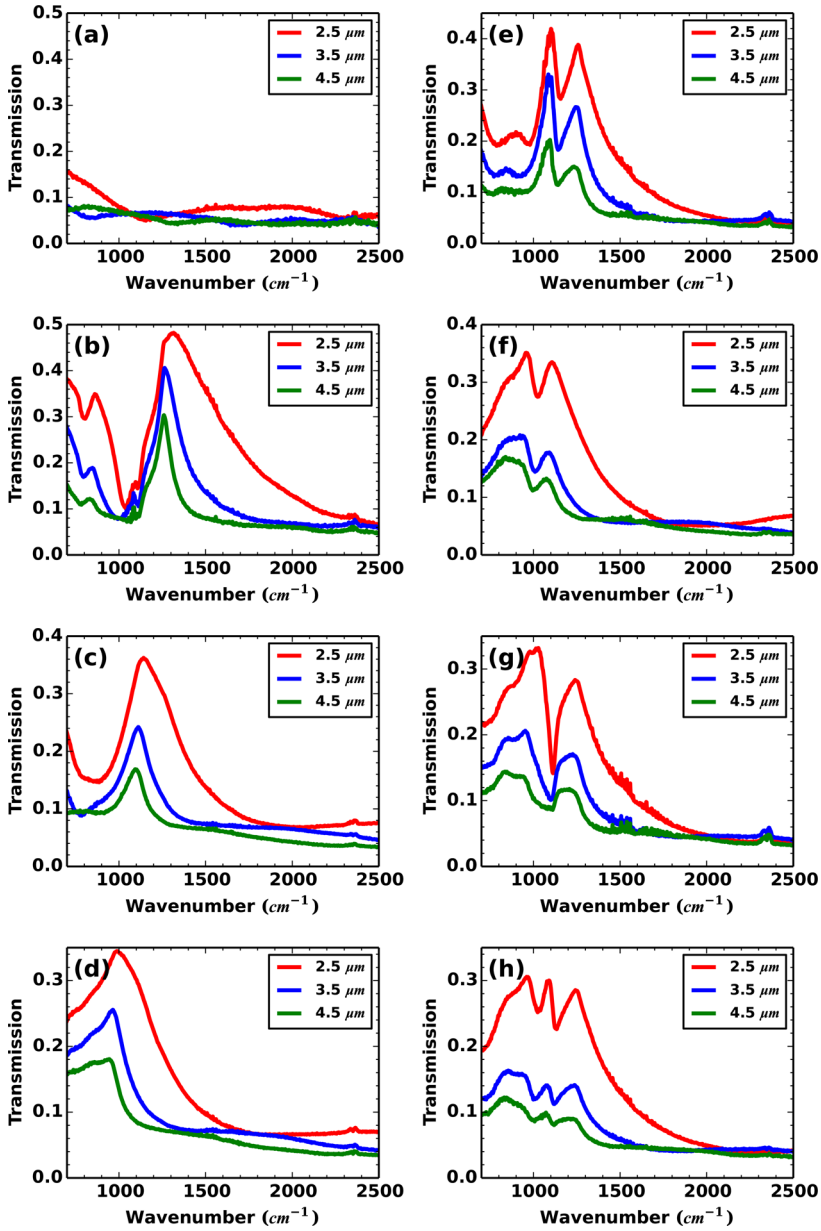

Figure 8. (a–d) Experimentally measured transmission spectra (a) without an epsilon-near-zero (ENZ) film with (b) SiO_2, (c) SiN, and (d) TiO_2. The thicknesses of the ENZ films are 300 nm. (e–h) Experimentally measured transmission spectra through the band-pass filters with various heterostructured ENZ films. Configurations and thicknesses of the films: (e) SiN, 300 nm; SiO_2, 300 nm; (f) TiO_2, 200 nm; SiN, 300 nm; (g) TiO_2, 200 nm; SiO_2, 300 nm; and (h) TiO_2, 150 nm; SiN, 150 nm; SiO_2, 300 nm. The legend represents the periods of the slit array.

the distance between the slits and ENZ films becomes a few hundred nanometers. This means that the near-field coupling is quite strong even in the presence of the air gap because the total thickness of the air gap and ENZ film lies in the subwavelength regime. When the air gap is filled by another ENZ material, such distant coupling can occur because the ENZ materials work as ordinary dielectric materials apart from the ENZ position. Therefore, the incident light can exclusively interact with a distant ENZ layer as well as an adjacent one due to the subwavelength nature of our ENZ heterostuructures. Namely, the strong distant coupling between the slits and ENZ film, as well as narrow ENZ bandwidth, allow for the construction of band-pass filters with ENZ heterostructures, which holds the mutually exclusive condition for the addition rule (Figure 6).

Meanwhile, the maximum transmission in Figure 7 monotonically decreases as the air gap becomes thicker for ENZ films with relatively high TO phonon wavenumbers (i.e., 833 to 1250 cm^{-1}). On the other hand, when using ENZ films with low TO phonon wavenumbers (i.e., 625 to 769 cm^{-1}), the maximum transmission slightly increases and then decreases. This might also be related to the fact that the positions of the resonance wavenumbers are proportional to the TO phonon wavenumbers (see the Figure 4a). In other words, a longer (shorter) wavenumber for a high (low) TO phonon ENZ film requires a larger (smaller) interaction length.

To support our simulation results, we performed experiments with natural ENZ materials, such as SiO_2 (ν_{LO} = 1250 cm^{-1}), SiN (ν_{LO} = 1150 cm^{-1}), and TiO_2 (ν_{LO} = 1000 cm^{-1}). The SiO_2, SiN, and TiO_2 films are grown using the thermal chemical vapor deposition (CVD), inductively coupled plasma

DOI: 10.1021/acsphotonics.6b00019
ACS Photonics 2016, 3, 819–827

chemical vapor deposition (ICPCVD), and sputter equipment, respectively. The filter structures were fabricated by the standard photolithography followed by the metal evaporation, and lift-off processes, whose dimensions were essentially the same as those of the simulations (Figure 1b); the metal thickness was 70 nm and slit width 500 nm. On the other hand, the thickness of the Si substrate (700 μm) was much larger than that of the simulation, and the period p varied from 2.5 to 4.5 μm. The conventional FT-IR (Fourier Transform InfraRed, Bio-Rad FTS 6000) system was employed to measure the transmission through our filters. The transmission without ENZ film (the slits were directly fabricated on the Si substrate) has no apparent peak and is less than ten percent in most spectral range (Figure 8a). When the various 300 nm thick ENZ films were inserted between the slits and substrate, strong resonance peaks were observed (Figure 8: (b) SiO_2, (c) SiN, and (d) TiO_2) at their ENZ positions. As the period decreased, the transmission increased owing to the increment of the coverage ratio (open area per total area), though the spectral shapes were preserved. This indicates that the resonant transmission characteristic was due to the ENZ effect rather than the geometrical effect. Finally, we constructed band-pass filters with various heterostructures of ENZ materials, Figure 8: (e) SiO_2/SiN, (f) SiN/TiO_2, (g) SiO_2/TiO_2, and (h) SiO_2/SiN/TiO_2. The detailed thicknesses and configurations are provided in the figure caption. From the wide transmission spectra in Figure 8e−h, it can be seen that the addition rule worked quite well in the real band-pass filters. In particular, three-layered heterostructures of the ENZ materials led to an ultrabroadband spectrum (Figure 8h).

Band-pass transmission spectra can be obtained using the resonance properties of the nanonatennas or metamaterials.[30−33] In this case, the multipass band can be achieved by closely packing the nanoantennas or meta-atoms of various sizes. However, due to the strong coupling between the adjacent elements, the transmissions as well as the resonance positions are significantly different from that for the isolated element. For example, Daniel Dregely et al. observed that the transmission through the vertically stacked nanoantennas was extensively different from that through the single nanoantenna.[34] Also, Muhan Choi et al. reported the photonic bandgap was formed as the number of metamaterial layers increased.[35] Therefore, we cannot construct the band-pass filters operating under the addition rule by combining the nanonatennas or metamaterials because the mutually exclusive condition does not hold. On the other hand, the slit structure itself does not support any resonance transmission when the thickness is small.[16,36,37] The sharp resonance transmission is only observed with the thick slits because of the Fabry−Perot effect.[38] As discussed in the Figure 2c,d, our slits are thin enough so that no transmission peaks are observed. In other words, the measured strong resonance peaks of our band-pass filters originate from the properties of the ENZ materials themselves, not a geometrical effect of the slit. Furthermore, the vertically stacked ENZ materials do not interact to each other holding the mutually exclusive condition. Consequently, apart from the vertically stacked nanoantennas or metamaterials, our heterostructured filters, slits on the multilayered ENZ materials, can work under the addition rule of probability keeping the transmission and resonance positions.

In conclusion, we have proposed a novel structure for band-pass filters operating under the addition rule of probability, instead of the multiplication rule. The slit array on the ENZ heterostructures allows for a multiband transmission spectrum, which behaves like the sum of the individual spectra. We performed various simulations and experiments to show that the mutually exclusive condition for the addition rule can be achieved by the narrow ENZ bandwidth and strong distant coupling of the slits and ENZ materials. The LC circuit model for the ENZ material has also been developed to explain the resonance characteristics of our band-pass filters. Through the success of this model, we can conclude that the ENZ film works as a capacitor when $n \geq k$, whereas it functions as an inductor when $n < k$. As an outcome of our study, we believe that additive-type band-pass filters can be used to construct ultrasensitive plasmonic biosensors or gas sensors.[39,40] Nowadays, broad-spectrum thermal sources are widely used in the mid-IR range to detect the numerous vibration modes of biological- or gaseous-molecules. In order to minimize noise and enhance detection efficiency, highly selective filters are required. Based on the additive coupling, we can easily design a filter that rejects the unwanted frequency bandwidth in order to raise the selectivity. Furthermore, an ENZ material constructed from visible metamaterials[41,42] could extend our study to the optical frequency range, which is essential in the context of Raman spectroscopy and fluorescence spectroscopy.

AUTHOR INFORMATION

Corresponding Author

*E-mail: jisoo.kyoung@samsung.com.

Notes

The authors declare no competing financial interest.

REFERENCES

(1) Stanley, R. Plasmonics in the mid-infrared. *Nat. Photonics* **2012**, *6*, 409−411.

(2) Editorial. Extending opportunities. *Nat. Photonics* **2012**, *6*, 407−407.

(3) Szeghalmi, A.; Helgert, M.; Brunner, R.; Heyroth, F.; Gösele, U.; Knez, M. Atomic layer deposition of Al_2O_3 and TiO_2 multilayers for applications as bandpass filters and antireflection coatings. *Appl. Opt.* **2009**, *48*, 1727−1732.

(4) Belyaev, B. A.; Tyurnev, V. V.; Shabanov, V. F. Design of optical bandpass filters based on a two-material multilayer structure. *Opt. Lett.* **2014**, *39*, 3512−3515.

(5) Fowles, G. R. *Introduction to Modern Optics*; Dover, 1989.

(6) Alu, A.; Bilotti, F.; Engheta, N.; Vegni, L. Metamaterial covers over a small aperture. *IEEE Trans. Antennas Propag.* **2006**, *54*, 1632−1643.

(7) Silveirinha, M.; Engheta, N. Tunneling of Electromagnetic Energy through Subwavelength Channels and Bends using ε -Near-Zero Materials. *Phys. Rev. Lett.* **2006**, *97*, 157403.

(8) Silveirinha, M. G.; Engheta, N. Transporting an Image through a Subwavelength Hole. *Phys. Rev. Lett.* **2009**, *102*, 103902.

(9) Adams, D. C.; Inampudi, S.; Ribaudo, T.; Slocum, D.; Vangala, S.; Kuhta, N. A.; Goodhue, W. D.; Podolskiy, V. A.; Wasserman, D. Funneling Light through a Subwavelength Aperture with Epsilon-Near-Zero Materials. *Phys. Rev. Lett.* **2011**, *107*, 133901.

(10) Inampudi, S.; Adams, D. C.; Ribaudo, T.; Slocum, D.; Vangala, S.; Goodhue, W. D.; Wasserman, D.; Podolskiy, V. A. ε -near-zero enhanced light transmission through a subwavelength slit. *Phys. Rev. B: Condens. Matter Mater. Phys.* **2014**, *89*, 125119.

(11) Choi, S. B.; Park, D. J.; Byun, S. J.; Kyoung, J.; Hwang, S. W. Near-Zero Index: Optical Magnetic Mirror for Field Enhancement and Subwavelength Imaging Applications. *Adv. Opt. Mater.* **2015**, *3*, 1719−1725.

(12) Ashcroft, N. W.; Mermin, N. D. *Solid State Physics*; Saunders College, 1976.

DOI: 10.1021/acsphotonics.6b00019
ACS Photonics 2016, 3, 819−827

(13) Hillenbrand, R.; Taubner, T.; Keilmann, F. Phonon-enhanced light-matter interaction at the nanometre scale. *Nature* **2002**, *418*, 159−162.
(14) Ocelic, N.; Hillenbrand, R. Subwavelength-scale tailoring of surface phonon polaritons by focused ion-beam implantation. *Nat. Mater.* **2004**, *3*, 606−609.
(15) Kyoung, J.; Park, D. J.; Byun, S. J.; Lee, J.; Choi, S. B.; Park, S.; Hwang, S. W. Epsilon-Near-Zero meta-lens for high resolution wide-field imaging. *Opt. Express* **2014**, *22*, 31875−31883.
(16) Seo, M. A.; Park, H. R.; Koo, S. M.; Park, D. J.; Kang, J. H.; Suwal, O. K.; Choi, S. S.; Planken, P. C. M.; Park, G. S.; Park, N. K.; Park, Q. H.; Kim, D. S. Terahertz field enhancement by a metallic nano slit operating beyond the skin-depth limit. *Nat. Photonics* **2009**, *3*, 152−156.
(17) Jeong, Y.-G.; Han, S.; Rhie, J.; Kyoung, J.-S.; Choi, J.-W.; Park, N.; Hong, S.; Kim, B.-J.; Kim, H.-T.; Kim, D.-S. A Vanadium Dioxide Metamaterial Disengaged from Insulator-to-Metal Transition. *Nano Lett.* **2015**, *15*, 6318−6323.
(18) Kim, J.-Y.; Kang, B. J.; Park, J.; Bahk, Y.-M.; Kim, W. T.; Rhie, J.; Jeon, H.; Rotermund, F.; Kim, D.-S. Terahertz Quantum Plasmonics of Nanoslot Antennas in Nonlinear Regime. *Nano Lett.* **2015**, *15*, 6683.
(19) Bahk, Y.-M.; Kang, B. J.; Kim, Y. S.; Kim, J.-Y.; Kim, W. T.; Kim, T. Y.; Kang, T.; Rhie, J.; Han, S.; Park, C.-H.; Rotermund, F.; Kim, D.-S. Electromagnetic Saturation of Angstrom-Sized Quantum Barriers at Terahertz Frequencies. *Phys. Rev. Lett.* **2015**, *115*, 125501.
(20) Kang, J. H.; Choe, J.-H.; Kim, D. S.; Park, Q. H. Substrate effect on aperture resonances in a thin metal film. *Opt. Express* **2009**, *17*, 15652−15658.
(21) Park, D. J.; C, S. B.; Ahn, Y. H.; Park, Q. H.; Kim, D. S. Theoretical Study of Terahertz Near-Field Enhancement Assisted by Shape Resonance in Rectangular Hole Arrays in Metal Films. *J. Korean Phys. Soc.* **2009**, *54*, 64.
(22) García-Vidal, F. J.; Moreno, E.; Porto, J. A.; Martín-Moreno, L. Transmission of Light through a Single Rectangular Hole. *Phys. Rev. Lett.* **2005**, *95*, 103901.
(23) Palik, E. D. *Handbook of Optical Constants of Solids*; Academic Press: San Diego, CA, U.S.A., 1998.
(24) Wang, L. P.; Zhang, Z. M. Resonance transmission or absorption in deep gratings explained by magnetic polaritons. *Appl. Phys. Lett.* **2009**, *95*, 111904.
(25) Lee, B. J.; Wang, L. P.; Zhang, Z. M. Coherent thermal emission by excitation of magnetic polaritons between periodic strips and a metallic film. *Opt. Express* **2008**, *16*, 11328−11336.
(26) Wang, L. P.; Zhang, Z. M. Phonon-mediated magnetic polaritons in the infrared region. *Opt. Express* **2011**, *19*, A126−A135.
(27) Dai, M.; Wan, W.; Zhu, X.; Song, B.; Liu, X.; Lu, M.; Cui, B.; Chen, Y. Broadband and wide angle infrared wire-grid polarizer. *Opt. Express* **2015**, *23*, 15390−15397.
(28) Engheta, N. Circuits with Light at Nanoscales: Optical Nanocircuits Inspired by Metamaterials. *Science* **2007**, *317*, 1698−1702.
(29) Chen, Y.-B.; Chiu, F.-C. Trapping mid-infrared rays in a lossy film with the Berreman mode, epsilon near zero mode, and magnetic polaritons. *Opt. Express* **2013**, *21*, 20771−20785.
(30) Brückner, J.-B.; Le Rouzo, J.; Escoubas, L.; Berginc, G.; Calvo-Perez, O.; Vukadinovic, N.; Flory, F. Metamaterial filters at optical-infrared frequencies. *Opt. Express* **2013**, *21*, 16992−17006.
(31) Strikwerda, A. C.; Zalkovskij, M.; Lund Lorenzen, D.; Krabbe, A.; Lavrinenko, A. V.; Uhd Jepsen, P. Metamaterial composite bandpass filter with an ultra-broadband rejection bandwidth of up to 240 terahertz. *Appl. Phys. Lett.* **2014**, *104*, 191103.
(32) Weber, D.; Albella, P.; Alonso-González, P.; Neubrech, F.; Gui, H.; Nagao, T.; Hillenbrand, R.; Aizpurua, J.; Pucci, A. Longitudinal and transverse coupling in infrared gold nanoantenna arrays: long range versus short range interaction regimes. *Opt. Express* **2011**, *19*, 15047−15061.
(33) Chen, H.-T.; Padilla, W. J.; Zide, J. M. O.; Gossard, A. C.; Taylor, A. J.; Averitt, R. D. Active terahertz metamaterial devices. *Nature* **2006**, *444*, 597−600.
(34) Dregely, D.; Taubert, R.; Dorfmuller, J.; Vogelgesang, R.; Kern, K.; Giessen, H. 3D optical Yagi-Uda nanoantenna array. *Nat. Commun.* **2011**, *2*, 267.
(35) Choi, M.; Lee, S. H.; Kim, Y.; Kang, S. B.; Shin, J.; Kwak, M. H.; Kang, K.-Y.; Lee, Y.-H.; Park, N.; Min, B. A terahertz metamaterial with unnaturally high refractive index. *Nature* **2011**, *470*, 369−373.
(36) Shalaby, M.; Merbold, H.; Peccianti, M.; Razzari, L.; Sharma, G.; Ozaki, T.; Morandotti, R.; Feurer, T.; Weber, A.; Heyderman, L.; Patterson, B.; Sigg, H. Concurrent field enhancement and high transmission of THz radiation in nanoslit arrays. *Appl. Phys. Lett.* **2011**, *99*, 041110.
(37) Novitsky, A.; Ivinskaya, A. M.; Zalkovskij, M.; Malureanu, R.; Uhd Jepsen, P.; Lavrinenko, A. V. Non-resonant terahertz field enhancement in periodically arranged nanoslits. *J. Appl. Phys.* **2012**, *112*, 074318.
(38) Lee, J. W.; Seo, M. A.; Kim, D. S.; Jeoung, S. C.; Lienau, C.; Kang, J. H.; Park, Q.-H. Fabry−Perot effects in THz time-domain spectroscopy of plasmonic band-gap structures. *Appl. Phys. Lett.* **2006**, *88*, 071114.
(39) Spagnolo, V.; Patimisco, P.; Borri, S.; Scamarcio, G.; Bernacki, B. E.; Kriesel, J. Mid-infrared fiber-coupled QCL-QEPAS sensor. *Appl. Phys. B: Lasers Opt.* **2013**, *112*, 25−33.
(40) Rodrigo, D.; Limaj, O.; Janner, D.; Etezadi, D.; García de Abajo, F. J.; Pruneri, V.; Altug, H. Mid-infrared plasmonic biosensing with graphene. *Science* **2015**, *349*, 165−168.
(41) Vesseur, E. J. R.; Coenen, T.; Caglayan, H.; Engheta, N.; Polman, A. Experimental Verification of $n = 0$ Structures for Visible Light. *Phys. Rev. Lett.* **2013**, *110*, 013902.
(42) Maas, R.; Parsons, J.; Engheta, N.; Polman, A. Experimental realization of an epsilon-near-zero metamaterial at visible wavelengths. *Nat. Photonics* **2013**, *7*, 907−912.

DOI: 10.1021/acsphotonics.6b00019
ACS Photonics 2016, 3, 819−827